AIP | The Journal of Chemical Physics

Freezing lines of colloidal Yukawa spheres. I. A Rogers-Young integral equation study

Jacek Gapinski, Gerhard Nägele, and Adam Patkowski

Citation: J. Chem. Phys. **136**, 024507 (2012); doi: 10.1063/1.3675607
View online: http://dx.doi.org/10.1063/1.3675607
View Table of Contents: http://jcp.aip.org/resource/1/JCPSA6/v136/i2
Published by the American Institute of Physics.

Freezing lines of colloidal Yukawa spheres. I. A Rogers-Young integral equation study

Jacek Gapinski,[1,a)] Gerhard Nägele,[2] and Adam Patkowski[1]
[1]*Faculty of Physics, A. Mickiewicz University, Umultowska 85, 61-614 Poznań, Poland*
[2]*Institute of Complex Systems (ICS-3), Forschungszentrum Jülich, D-52425 Jülich, Germany*

(Received 5 August 2011; accepted 16 December 2011; published online 13 January 2012)

Using the Rogers-Young (RY) integral equation scheme for the static structure factor combined with the one-phase Hansen-Verlet (HV) freezing rule, we study the equilibrium structure and two-parameter freezing lines of colloidal particles with Yukawa-type pair interactions representing charge-stabilized silica spheres suspended in dimethylformamide (DMF). Results are presented for a vast range of concentrations, salinities and effective charges covering particles with masked excluded-volume interactions. The freezing lines were obtained for the low-charge and high-charge solutions of the static structure factor, for various two-parameter sets of experimentally accessible system parameters. All RY-HV based freezing lines can be mapped on a universal fluid-solid coexistence line in good agreement with computer simulation predictions. The RY-HV calculations extend the freezing lines obtained in earlier simulations to a broader parameter range. The experimentally observed fluid-bcc-fluid reentrant transition of charged silica spheres in DMF can be explained using the freezing lines obtained in this work. © *2012 American Institute of Physics*. [doi:10.1063/1.3675607]

I. INTRODUCTION

A wide class of industrially and biologically relevant dispersions of charge-stabilized colloidal particles of globular shape[1–6] can be described by a repulsive Yukawa-type effective pair energy of the form[7]

$$\beta u(r) = L_B Z^2 \left(\frac{e^{\kappa a}}{1+\kappa a}\right)^2 \frac{e^{-\kappa r}}{r}, \qquad r > \sigma = 2a \tag{1}$$

in combination with an excluded-volume interaction characterized by the hard-sphere diameter σ. Here, $\beta = 1/(k_B T)$ with Boltzmann constant k_B and temperature T, r is the center-to-center separation of two spheres, $L_B = e^2/(\varepsilon\ k_B T)$ is the Bjerrum length of the suspending fluid of dielectric constant ε, and Z is the effective number of elementary charges, e, on a colloidal particle. The Debye screening parameter, κ, is given by[7]

$$\kappa^2 = \frac{4\pi L_B\,[n\,|Z| + 2C_s]}{1-\phi}. \tag{2}$$

It comprises a contribution from (monovalent) counterions released from the surfaces of colloids with number density n, and a contribution from the co- and counterions of an added 1-1 electrolyte of number density C_s. The factor $1/(1-\phi)$, where $\phi = (4\pi/3)na^3$, is the colloid volume fraction, corrects for the free volume accessible to the small microions. This Yukawa-type pair energy captures essential features of charge-stabilized suspensions, for systems where the short-range van der Waals attractions can be neglected. For a stable suspension, the electrostatic repulsion is strong enough to prevent contact configurations, i.e., rendering them extremely unlikely, so that the excluded volume interactions are of no consequence. Well-studied experimental systems which fall into this category are (sulfonate) polystyrene latex spheres in water[8,9] or in an ethanol-water mixture,[3,4] silica and polymethylacrylate (PMMA) spheres in an organic solvent (mixture),[6,10,11] and to some extent also charged globular proteins in water such as apoferritin[12,13] or bovine serum albumin (BSA).[14,15]

The pair potential in Eq. (1) depends on four dimensionless parameter groups $\{L_B/\sigma\ ,\ Z\ ,\ C_s\sigma^3\ ,\ \phi\}$, which can be controlled experimentally to a larger extent. However, the important subclass of systems with masked hard-core interactions is completely characterized by two independent parameters only.[16] A convenient choice of these parameters for theoretical discussions is[16]

$$\lambda = \kappa\ \langle r\rangle\ , \tag{3}$$

$$\tilde{T} = \frac{k_B T}{u\,(\langle r\rangle)}, \tag{4}$$

where λ is the geometric (simple-cubic) mean particle distance, $\langle r\rangle = n^{-1/3}$, expressed in units of the Debye screening length κ^{-1}, and $\tilde{T}$ measures the thermal energy relative to the potential energy, $u(\langle r\rangle)$, of a pair of particles at distance $r = \langle r\rangle$. Different combinations of the four parameters $\{L_B/\sigma\ ,\ Z\ ,\ C_s\sigma^3\ ,\ \phi\}$ sharing the same fluid-phase state point $\{\lambda, \tilde{T}\}$ also share the same static structure factors, $S(q)$, and radial distribution functions (rdf), $g(r)$, for the scattering wavenumber q and pair distance r measured in units of $\langle r\rangle$.[17,18]

The universal $\lambda - \tilde{T}$ phase diagram of these effectively point-like Yukawa particles is quite simple, and has been well explored over the past 20 years.[16,17,19–27] It consists of a single (supercritical) fluid phase that can freeze into an fcc or a bcc

a)Electronic mail: gapinski@amu.edu.pl.

solid, characterized by 8 or 12 next neighbor particles, respectively. The phase diagram has a single triple point but no critical point, since the pair interactions in this one-component system are purely repulsive.

Note that the extended phase diagram not considered in the present work, where the $g(r)$ of hard-sphere-Yukawa particles is allowed to be discontinuous at contact distance, $r = \sigma$, is more complicated, showing an additional fluid-fcc-bcc triple point.[17,23,27] Moreover, a third parameter, namely, the volume fraction ϕ, is then required in addition to λ and $\tilde{T}$, to fully characterize the phase behavior and static pair correlations. If the hard core matters physically, in actual suspensions of charged particles one needs to consider then the attractive van der Waals forces which tend to destabilize the system, changing the phase behavior away from that of a pure hard-sphere Yukawa system.

The aim of this paper is to provide a thorough theoretical exploration of two-parametric liquid-solid freezing lines in colloidal Yukawa-particle systems with masked excluded volume interactions, for a wide range of experimentally adjustable control parameters such as the particle volume fraction, effective charge, and the added salt concentration. For each discussed two-parameter freezing line diagram, the third parameter is varied over a very broad range of values. The present work should thus prove helpful to experimentalists who plan to perform experiments on concentrated charge-stabilized suspensions near to a freezing transition. The user-friendly freezing line diagrams discussed in this paper, which are expressed in terms of experimental control parameters, are not deducible in general from the universal $\tilde{T}-\lambda$ phase diagram, due to the aforementioned non-reciprocal mapping from $\{L_B/\sigma\ ,\ Z\ ,\ C_s\sigma^3\ ,\ \phi\}$ to $\{\lambda, \tilde{T}\}$.

The extensive parameter scans presented here have been obtained using the accurate Rogers-Young (RY) integral equation scheme in combination with the fluid-phase Hansen-Verlet (HV) rule for the principal peak height, $S_f(q_m)$, of the static structure factor $S(q)$ at freezing. Here, q_m is the scattering wavenumber reciprocally related to the size of the next-neighbor cage formed around each particle.[7,28] The HV criterion is a semi-empirical rule found in computer simulations on atomic liquids and colloidal fluids. It can be motivated by the density-wave mean field theory of freezing, according to which a fluid approaching freezing becomes increasingly unstable against spontaneous density modulations of wave vectors of magnitude near q_m which at freezing change the uniform fluid density profile to the periodic profile of the crystal.[29,30]

The RY-HV method allows for a conveniently fast, and as we will show in comparison to the universal $\tilde{T}-\lambda$ diagram, quite accurate calculation of freezing lines in various parameter representations. A detailed study of experimental-parameter freezing lines on the basis of computer simulations or elaborate density functional theory calculations of similar generality as the one presented here, would have been numerically very expensive and time consuming. We show that the fast RY-HV method predicts a universal freezing line in the $\lambda - \tilde{T}$ phase-space in good overall agreement with simulation results by Stevens and Robbins,[22] Meijer and Frenkel,[20] and Hamaguchi *et al.*,[23] however, extending these earlier results to substantially larger values of λ. Note here again that, while $\lambda - \tilde{T}$ phase space considerations are important from a theoretical viewpoint, the experimentally controllable parameters such as salt concentration and effective charge cannot be uniquely determined from λ and $\tilde{T}$ alone. The good agreement justifies our usage of the RY-HV scheme in studying various structural properties under freezing conditions. As an interesting experimental result, we will show that the most recent and most accurate Yukawa spheres simulation result by Hamaguchi *et al.*[23] for the bcc−fcc coexistence line, which is located in $\tilde{T}-\lambda$ phase space noticeably away from the one predicted by Robbins *et al.*,[16] and for the bcc phase region extending to λ values substantially larger than the one in Ref. 16 is fully consistent with our x-ray scattering data for silica spheres in DMF.

For neutral hard spheres, one finds $S_f(q_m) = 2.85$ at freezing.[31] For the charge-stabilized colloidal systems with soft Yukawa repulsion studied in this work, where the hard core plays no physical role, a constant value of $S_f(q_m) = 3.1$ is used. This value is in agreement with the experimental peak height obtained from our x-ray scattering experiments on coated, charge-stabilized silica spheres suspended in DMF,[10] and conforms to computer simulation results,[19,22] and density functional theory calculations,[25,26] where for masked-core Yukawa particles freezing values of $S_f(q_m)$ around 3 have been reported. According to our calculations, the two-parametric freezing lines do not change appreciably when the HV peak value is altered by ± 0.1. The present work on thermodynamic and structural freezing lines complements related theoretical work on short-time diffusion in silica-DMF suspensions.[32] In this earlier work, the same HV freezing value of 3.1 was used in deriving a universal limiting freezing line for the peak height of the hydrodynamic function, a quantity central to dynamic scattering experiments in the colloidal short-time regime.

We emphasize here that the thermodynamically self-consistent RY integral equation scheme is required to obtain precise values for the effective particle charge. Usage of a less accurate scheme such as the analytical rescaled mean spherical approximation (RMSA) might for a number of systems even lead to a failure in predicting a freezing transition. Very recently, an improved variant of the RMSA for hard-sphere Yukawa fluids has been derived, referred to as the modified penetrating-background-corrected RMSA (MPB-RMSA, for short),[18] which combines the analyticity of the RMSA solution for $S(q)$ with a strongly improved accuracy. However, different from the RY scheme, the MPB-RMSA is thermodynamically not self-consistent and somewhat less accurate in its predictions for $g(r)$. Therefore, we use here the RY scheme for the price of a larger numerical effort.

As we have already discussed in earlier works,[10,32] for the Yukawa pair potential in Eq. (1) there exist two separated branches of effective charge values with pairwise very similar static structure factors in each branch which can be hardly distinguished experimentally. The existence of these two solutions has been overlooked in many earlier applications. To gain a complete survey on two-parameter freezing lines, both the low-charge branch and high-charge branch solutions for $S(q)$ have been determined and discussed, on pointing to

differing trends which allow for distinguishing these solutions. Our discussion should prove helpful in deciding which of the two solutions (i.e., which of the two in general largely different effective charge numbers) is the physical one for the system under study.

The present paper is not concerned with the on-going discussion on how the effective charge, Ze, in Eq. (1) is quantitatively related to a bare particle charge, commonly referred to as the colloid charge renormalization problem. The bare charge is usually defined on a more fundamental, so-called Primitive Model level of description where the colloidal particle and the microions are treated equally as uniformly charged spheres of different sizes. Poisson-Boltzmann type cell model,[33] renormalized jellium model methods,[34–36] and non-mean-field generalizations accounting for the effect of multivalent microions,[37] have been derived which allow for calculating the effective charge approximately as a function of volume fraction, salt concentration, and bare colloid charge. Noteworthy here is a recent phase diagram calculation[36] for Yukawa spheres with built-in (approximate) charge renormalization, for particles at constant zeta potential. We refrain here from including charge-renormalization into our quantitative analysis of freezing lines, not only for maintaining the paper in an acceptable size, but also since the calculated renormalized charge values can differ substantially, depending on the charge renormalization method and the invoked chemical charge regulation scheme.

We are also not dealing here with the exploration of non-pairwise additivity effects in the electrostatic interactions which can play a role for $\lambda \leq 2$, i.e., for deionized suspensions of comparatively large particle concentrations.[17]

The present paper (labeled I) focuses on the construction and discussion of freezing lines in terms of experimentally accessible parameters. In a related forthcoming paper by the same authors (labeled II), we will discuss the behavior of pair energies at freezing in relation to characteristic features in $S(q)$ and $g(r)$.

The paper is organized as follows: Sec. II summarizes our method of calculating freezing lines for different system parameters. Numerical and experimental results and discussion for the freezing lines are presented in Sec. III. RY-HV construction of freezing lines is presented in Subsection III A. Differences in the low-charge (LZ) and high-charge (HZ) solutions of the RY scheme are discussed in Subsection III B. Three sets of two-parameter freezing lines are presented in Subsection III C. In subsection III D, the RY-HV predicted universal freezing line in the $\lambda - \tilde{T}$ space is compared to simulation predictions by different groups. The salt-induced fluid-bcc-fluid reentrant transition is investigated in Subsection III E. Our conclusions are given in Sec. IV.

II. METHOD OF CALCULATION AND EXPERIMENTAL DETAILS

In this paper, we provide a detailed theoretical exploration of two-parameter freezing lines for monovalent colloidal Yukawa spheres of pair interaction according to Eq. (1), with masked excluded volume interactions. The particle diameter and the solvent properties have been selected to describe charged silica spheres suspended in dimethylformamide (DMF). Our results cover a broad range of volume fractions ϕ, 1-1 electrolyte concentrations C_s, and effective particle charge numbers Z. We discuss the form of the freezing lines for different pairs of the experimentally controllable parameters ϕ, C_s, and Z.

The freezing lines are obtained using the standard RY integral equation method for the static structure factor $S(q)$, in combination with the HV freezing rule for its principal peak height. Since we are concerned here with the important class of charge-stabilized systems where the particle hard-core plays no physical role, a constant peak height value of $S_f(q_m) = 3.1$ is used to characterize the onset of freezing into a crystalline state. The employed RY method is a hybrid method which interpolates continuously between the Percus-Yevick closure at small, and the hypernetted chain closure at long distances, by a single-parameter mixing function. The mixing parameter is determined by imposing local thermodynamic consistency, i.e., by enforcing equality between the isothermal compressibilities derived from the compressibility and virial (pressure) equation of states. For details see Ref. 38. The RY method has been found, from numerous comparisons with simulation results for $S(q)$ and $g(r)$ (see, e.g., Refs. 18 and 39), to perform excellently for the (three-dimensional) hard-sphere plus repulsive Yukawa pair potential. Note that in this work we use the RY method solely to calculate the pair correlation functions, not addressing the thermodynamic subtleties which one faces for systems with state-dependent pair potentials.

The system parameters employed in the theoretical calculations represent suspensions of monodisperse silica spheres of diameter $\sigma = 2a = 171$ nm and mass density $\rho = 1.95$ g/cm^3 in DMF ($\varepsilon = 36.7$ at $T = 20$ °C, Bjerrum length $L_B = 1.55$ nm), and subjected to a broad range of added LiCl concentrations. Different from aqueous suspensions, this well-characterized system is not plagued by uncontrolled CO_2 contamination and self-dissociation of water molecules. Therefore, systems with very low salinities can be prepared. For our silica in DMF system, we have obtained a large body of static and short-time dynamic x-ray scattering data, for systems in the fluid-phase regime.[10] The small-angle x-ray scattering (SAXS) measurements were performed at the European Synchrotron Radiation Facility (ESRF) in Grenoble using synchrotron radiation at Troika III part of the ID 10A beamline in cooperation with the coauthors of Ref. 10. The experimental details concerning the beamline and sample preparation are given in Ref. 10.

III. RESULTS AND DISCUSSION

A. RY-HV construction of freezing lines

We consider first salt-free suspensions, characterized by a tiny residual amount, $C_s = 1\times10^{-9}$ M, of added 1-1 electrolyte (e.g., LiCl).

Figures 1(a) and 2(a) show concentration series of the RY-calculated static structure factor, obtained on assuming a concentration-independent effective charge number of $Z = 300$ and 5000, respectively, in units of the proton charge e. As can be noticed from these figures, the shape of $S(q)$

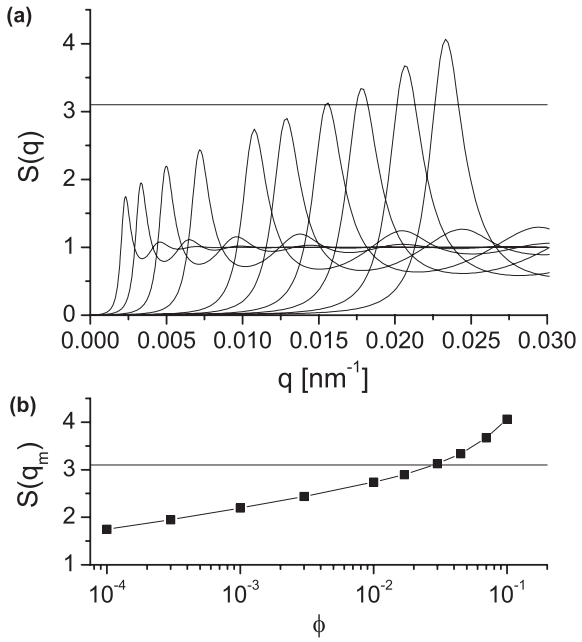

FIG. 1. (a) RY-calculated static structure factor, $S(q)$, for salt-free suspensions at different volume fractions $\phi = 0.0001$, 0.0003, 0.001, 0.003, 0.01, 0.017, 0.03, 0.045, 0.07, 0.1 (from left to right), and constant low-charge value $Z = 300$. (b) The principal peak height, $S(q_m)$, as a function of ϕ. The horizontal lines mark the HV value, $S(q_m) = 3.1$, used throughout this paper as indicator for the onset of freezing.

with increasing volume fraction depends strongly on the effective charge number. For the low charge value in Figs. 1(a) and 1(b), the principal maximum, $S(q_m)$, of $S(q)$, located at the wavenumber position q_m, increases monotonically with increasing ϕ (more weakly so at lower concentrations), with the peak position shifting to larger wavenumbers. Observe here in Fig. 1(b) the linear–log scale. The horizontal line representing $S_f(q_m) = 3.1$ indicates the Hansen-Verlet threshold value at which a Yukawa-type system with masked excluded volume interactions is about to freeze into a bcc or fcc solid phase. The structure factors with $S(q_m) > 3.1$ should be considered as mere analytic extensions of the fluid-phase structure factors into a region, where the colloidal system is not fluid any more. In the following, we will use some of those "virtual" points for discussion or illustration, but keeping in mind that they do not represent the real state of the system.

Different from Fig. 1, at very high effective charge values like the one considered in Fig. 2, $S(q_m)$ becomes a highly non-monotonic function in ϕ. For very small concentrations, the peak height increases initially, traversing the freezing line at $\phi \approx 5\times10^{-8}$, subsequently passing through a high maximum (not resolved on the scale of Fig. 2(b)) which is located in the non-fluid volume fraction regime. When ϕ is further increased, a reentrant fluid phase is found according to the HV rule, in a concentration window of $0.0045 < \phi < 0.11$. For $\phi > 0.11$, the system freezes again.

The volume fraction dependence of $S(q_m)$ in a "salt-free" suspension (at $C_s = 10^{-9}$ M) is shown in Fig. 3, for a series of effective charges ranging from low values (solid lines) to high-charge values (dashed lines). The intersection of the horizontal line, defined by $S_f(q_m) = 3.1$, with the iso-charge curves gives the freezing transition points.

The concentration window where the reentrant solid-fluid-solid transition occurs (for charge numbers $Z > 3500$ in the case of salt-free systems), broadens with increasing Z, while the primary fluid-phase regime (starting from $\phi = 0$) is narrowed to very small values of ϕ.

Similar calculations of $S(q_m)$ have been performed also for several values of added salt concentration C_s. A summary of these results is shown in Fig. 4. In Fig. 4(a), results for $S(q_m)$ are presented using a constant charge number of

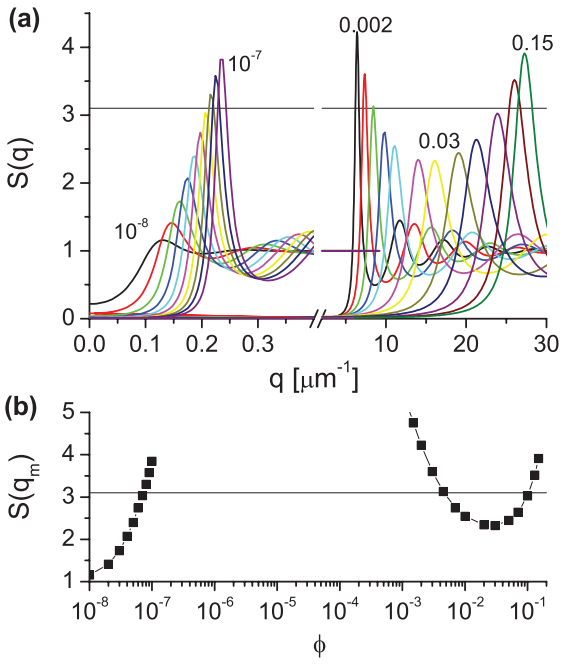

FIG. 2. (a) RY static structure factor for "salt-free" suspension at volume fractions $\phi = 1\times10^{-8}$, 2×10^{-8}, 3×10^{-8}, 4×10^{-8}, 5×10^{-8}, 6×10^{-8}, 7×10^{-8}, 8×10^{-8} (left group) and $\phi = 0.002$, 0.003, 0.0045, 0.007, 0.01, 0.02, 0.03, 0.05, 0.07, 0.1, 0.13, 0.15 (right group), using a large effective charge value of $Z = 5000$. (b) Principal peak height $S(q_m)$ as a function of ϕ plotted on a linear-log scale. The horizontal lines mark the HV value, $S(q_m) = 3.1$, used throughout this paper as indicator for the onset of freezing.

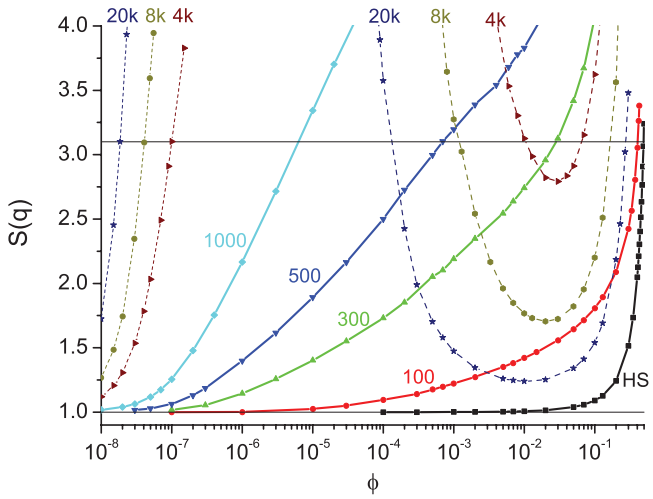

FIG. 3. RY static structure factor peak height, $S(q_m)$, as a function of ϕ, for values of Z as indicated (1k = 1000), and constant $C_s = 0.001$ μM. Solid lines are for Z values in the small-charge region $Z = 0$–1000. The dashed lines are the high-charge region results for $Z = 4000$–20 000.

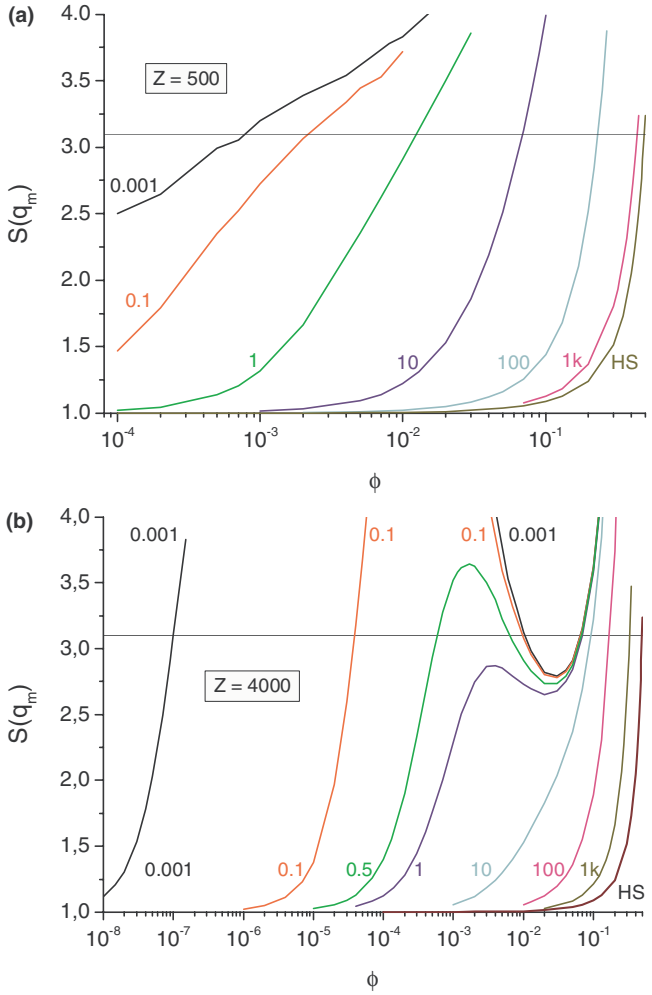

FIG. 4. Added salt concentration dependence of $S(q_m)$, (a) for a low-charge value of $Z = 500$, and (b) for a high-charge value of $Z = 4000$. The numbers at the solid curves are the salt concentrations, C_s, in μM (1k = 1000). The lowest curves in (a) and (b), labeled by HS, represent the neutral hard-sphere results. Horizontal lines: $S(q_m) = 3.1$.

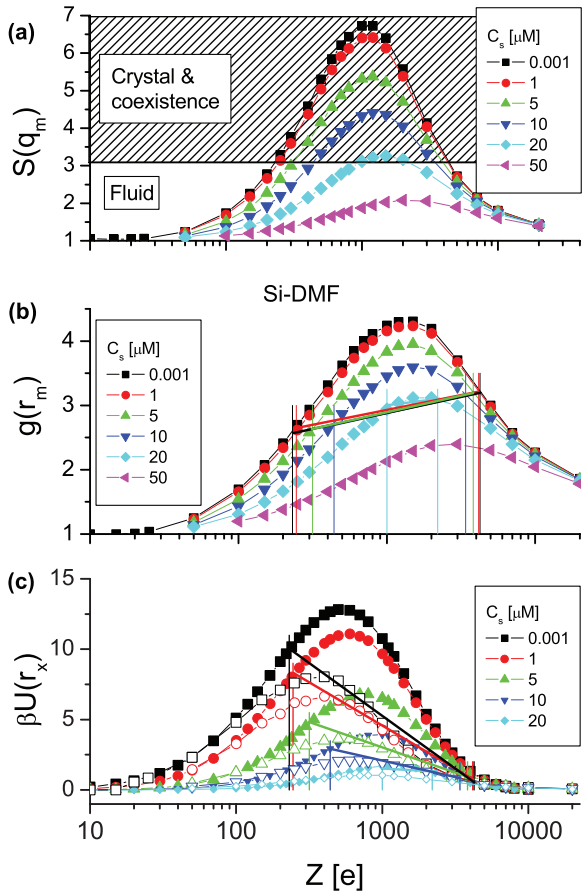

FIG. 5. Z-dependence of (a) the static structure factor maximum $S(q_m)$, (b) the radial distribution function maximum $g(r_m)$, and (c) the pair interaction energy at $r_x = \langle r \rangle$ (solid symbols) and at $r_x = r_m$, (open symbols) calculated using the RY scheme for $\phi = 0.077$, and added salt concentrations as indicated. Here, r_m, is the distance where $g(r)$ attains its maximum. The equally colored vertical line pairs in (b) and (c) denote the low-charge and the high-charge values of Z for a given C_s where the freezing condition $S(q_m) = 3.1$ is met. The inclined solid line segments in (b) and (c) connect the freezing points of the corresponding low-charge and high-charge pairs.

$Z = 500$, representative of the "low charge" behavior (monotonic increase in $S(q_m)$), for six values of added salt concentration (0.001 μM to 1000 μM in decade steps). The line obtained for the largest C_s is almost identical to the one describing a neutral hard-sphere system, whose $S(q_m)$ is also shown in the figure. In Fig. 4(b), we demonstrate how the addition of salt affects the behavior of a system at $Z = 4000$e, which is a representative high-charge value for low-salt systems. The non-fluid phase region for intermediate values of ϕ, which is very broad for small C_s, narrows with increasing salt concentration and disappears for 0.5 μM $< C_s <$ 1 μM, although the non-monotonic behavior of $S(q_m)$ as a function of ϕ is still visible for $C_s \approx 1$ μM. Contrary to the low-charge case, a concentration of 1 mM added salt is not yet sufficient to reach the hard-sphere behavior.

B. Low- and high-charge RY solutions

An interesting observation made in Fig. 3 is that for many systems of a given volume fraction and salt concentration, the same structure factor peak height is obtained for two very different effective charge values (see the crossing points of solid and dashed curves). To study this finding in more detail, in Fig. 5(a) we plot $S(q_m)$ as a function of Z, for a volume fraction $\phi = 0.077$ and various salt concentrations. The peak height of $S(q)$ as a function of Z passes through a maximum located roughly in between $Z = 1000$ and 2000. For low salt-content, this maximum is located, according to the HV rule, in the non-fluid regime. Thus, a reentrant fluid–solid–fluid transition is described for increasing Z. The fluid-phase charge-number regions to the left and right of the maximum in $S(q_m)$ are referred to, respectively, as the low-charge and high-charge regions. In the low-charge (high-charge) region, $S(q_m)$ increases (decreases) with increasing Z. The width of both regions grows with increasing salinity. At a sufficiently large salinity, of value depending on the particle concentration, the two disjoint fluid-state regions merge into a single one, describing systems that do not freeze into a solid for any value of the effective charge (at this particular volume fraction). For a proper description of this merging, it is crucial to use an accurate integral equation method such as the RY scheme. Using a less accurate scheme such as the regularly applied

analytic RMSA, or the numerical hypernetted chain approximation (HNC), which both underestimate the particle ordering to some extent, could result in the prediction of the absence of a freezing transition for systems where freezing actually takes place. Moreover, precise integral equation methods, such as the RY scheme and the MPB-RMSA scheme,[18] are necessary to obtain accurate values for the effective charge.

For the systems regarded in Fig. 5(a), the maximum of $S(q_m)$ is located in between $Z = 1000$ and 2000, with its position shifting to larger charge values for larger salt concentrations. Comparing this to Fig. 3, where zero-salt systems are considered for fixed values of Z, and where $S(q_m)$ traverses a maximum as a function of ϕ, when the surface-counterion contribution to $\kappa_{ci}^2 \propto \phi$ becomes sufficiently strong to overcompensate the ordering effect caused by the increasing particle concentration. When ϕ in Fig. 3 is further increased for a large-Z system, $S(q_m)$ passes through a minimum observed at $\phi \sim 0.01$–0.1. The upswing of $S(q_m)$ at the largest considered ϕ values located to the right of this minimum is due to the proximity of next-neighbor particles which are subject to a sharply rising pair energy.

Figure 5(b) shows the principal peak height, $g(r_m)$, of the radial distribution function (rdf) as a function of Z, for the same systems as in Fig. 5(a). The vertical line pairs of equal color indicate, for a given salt concentration, corresponding low-charge and high-charge values of Z where the criterion $S(q_m) = 3.1$ is fulfilled. The Z-interval in between a vertical line pair describes a non-fluid region. The height of $g(r_m)$ at freezing is different for the low-charge and the high-charge systems, i.e., $g_f(r_m)_{\text{high}} > g_f(r_m)_{\text{low}}$. The relative difference decreases with increasing salt content. Thus, there is no simple overall mapping of the HV freezing criterion for the structure factor peak height to a comparatively simple criterion in terms of $g_f(r_m)$. A single value for $S_f(q_m)$ corresponds in general to a broader range of values for $g_f(r_m)$ (see also Ref. 18). The peak values $g_f(r_m)$ for the entire range of the system parameters will be thoroughly discussed in a related paper (labeled II).

The Z-dependence of $u(\langle r \rangle)$ and $u(r_m)$, for a constant ϕ and C_s varying from 10^{-9} M to 20 μM, is analyzed in Fig. 5(c). Even though r_m is very close to $\langle r \rangle$ in low-salinity systems, the pair interaction energy changes so rapidly with distance that a slightly larger r_m results in a distinctly lower value of the pair energy, and in the maximum of $u(r_m)$ shifted to a smaller value of Z. The maximum of $S(q_m)$ as a function Z in Fig. 5(a), is reflected by a corresponding maximum of $u(r_m)$ which is located, however, at a smaller value of Z. The maximum reflects the counterplay of the electric coupling strength, $\beta u(\sigma^+)$, and the counterion screening. The latter dominates for large Z values. The vertical line pairs in Fig. 5(c) indicate the low-charge and high-charge values where freezing takes place. A fluid phase is found only outside these charge interval boundaries (bounded by the vertical lines). The pair energy at freezing is distinctly different for the low-charge and high-charge values. This points to the impossibility of formulating a freezing criterion in terms of $u(r_m)$ alone. The same degree of fluid ordering as quantified by $S(q_m)$ can be obtained for two distinctly different pair interaction energies. The behavior of $g_f(r_m)$ and $\beta u(r_x)$ at freezing will be discussed in detail in a related forthcoming paper (labeled II).

At this point, one should consider the physical relevance of the high-charge solutions for $S(q)$ and $g(r)$. Whether a high-charge solution is physically relevant depends on the system under consideration. There are limits to the maximal value the effective charge can attain in charge-stabilized suspensions set by the quasi-condensation of counterions (charge-renormalization effect), and by chemical charge regulation when weakly acid surface groups are present. As noted in Sec. I, estimates of the effective particle charge can be obtained from approximate Poisson-Boltzmann calculations with radial symmetry[33,35,36] and generalizations to multivalent microions.[37] The smallest values for the saturated effective charge number, Z_{sat}, are found at low salinity. We note here that Z_{sat} increases significantly with increasing salt concentration. For the silica in DMF suspensions studied in,[10] effective charge values $Z \leq 2500$ have been obtained from electrophoretic dynamic light scattering measurements performed on highly diluted samples. For the same salt concentrations values of $Z < 10^4$ in the low charge branch were obtained from the RY fits to the experimental $S(q)$ in the fluid regime at ϕ of the order of 0.1. In both the cases, the Z values were increasing with increasing salt concentration. According to Fig. 4(a), the range of allowed effective charge values extends appreciably into the high-charge region. Thus, the high-charge solutions are included into our discussion not only for completeness, but also since they can be of relevance for systems at higher salinity. Moreover, their discussion serves to point to the still largely unknown fact that there are two quite similar solutions for $S(q)$ with distinctly different effective charges.

C. Two-parameter freezing lines

The phase behavior of suspensions of charge-stabilized colloidal spheres depends, for given particle size and solvent properties, on the effective charge number Z, colloid volume fraction ϕ, and added salt concentration C_s. Since the corresponding three-dimensional phase diagram would be cumbersome to display, in the following we focus on two-dimensional phase diagram sections, obtained from varying two system parameters while keeping the third one constant.

From the experimental point of view, C_s and ϕ are in general well-controlled parameters. However, even these parameters cannot be precisely determined: the volume fraction at a particular position in the sample might differ from its nominal value in systems with non-negligible sedimentation, and the ionic strength in aqueous suspensions can change in an uncontrolled way due to CO_2 molecules dissolved in water and forming carbonic acid. To avoid the latter problem, in our experiments we use DMF as the suspending solvent. The effective particle charge Z is determined by the RY fit to the experimental structure factor peak height. The effective charge depends on C_s and ϕ typically in an involved way through a general $Z = Z(L_B Z/a, \kappa a, \phi)$ dependence. For this reason, the iso-Z freezing lines we are going to discuss in the following do not directly correspond to an actual experimental system.

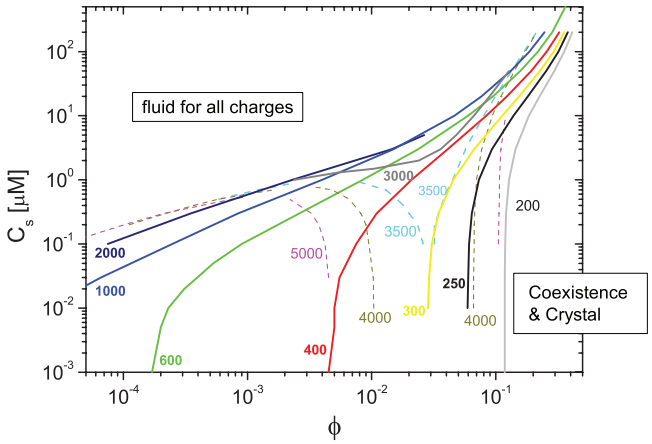

FIG. 6. $C_s-\phi$ phase diagram for a charge series of iso-charge freezing lines, predicted using the RY scheme with $S_f(q_m) = 3.1$. Solid lines: low-charge freezing lines for charge values as indicated. Dashed lines: high-charge freezing lines.

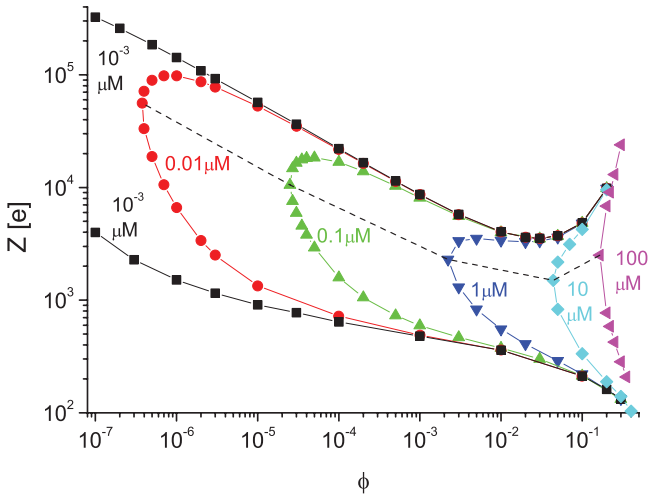

FIG. 7. Iso-C_s freezing lines in the Z–ϕ phase calculated using the H-V criterion. The selected C_s values are indicated in the figure. The dashed line connects points on the iso-C_s lines fulfilling the condition $Z_{low} = Z_{high}$.

However, an experimental freezing line characterizing a concentration series can be easily constructed from a family of iso-charge freezing lines.

In Fig. 6, we show the $C_s-\phi$ phase diagram with a family of iso-Z freezing lines obtained from the RY scheme in combination with the HV freezing rule. The freezing lines for low-charge values (solid curves) increase monotonically in ϕ, indicating that systems of larger salinity solidify at larger concentrations. With increasing Z in the low-charge region, the freezing lines move upwards, most strongly so at very small volume fractions. Accordingly, the area of the fluid-phase region extending into the upper left part of the phase diagram becomes smaller.

When the effective charge is increased above $Z \approx 1000$, the iso-charge freezing lines become non-monotonic for $Z = 3300$–3400 (these lines are not shown in the figure), bending down at intermediate ϕ values towards the lower right corner of the diagram until, at $Z \approx 3500$, the lines become discontinuous and a reentrant transition is predicted: For constant salinity of $C_s < 1$ μM, a reentrant fluid-solid-fluid-solid transition sequence is traversed with growing ϕ. This transition sequence occurs for large particle charges and at very low salinity. It is due to the interplay of the pair energy contact value and the surface-counterions screening, which both become larger with increasing ϕ. The $C_s-\phi$ phase space behavior of the freezing lines in the high-charge region differs qualitatively from that in the low-charge region. For example, in the high-charge case the fluid-phase area is growing with increasing Z. For $C_s > 1$ μM, no reentrant transition sequence is observed any more and only the right-hand branch of the high-charge freezing line is accessed. Different from the low-charge case, freezing lines are shifted to larger concentrations when Z is increased. Thus, a putative high-charge crystal melts when the charge is increased. At this point, it should be pointed out again that the employed HV criterion lacks the sensitivity to distinguish a fluid-bcc from a fluid-fcc freezing transition.

From the experimental point of view, another convenient way to present the phase diagram of a Yukawa-like colloidal system is to use iso-ϕ freezing lines in the (Z–C_S) and iso-C_S freezing lines in the ($Z-\phi$) coordinates. The (Z–ϕ) phase diagram is presented in Fig. 7. In this figure, freezing lines for different constant C_S are shown which define values of Z and ϕ at freezing for a Yukawa system.

Here, one clearly sees that at high ϕ all iso-C_s freezing lines both for the low- and high-charge branches collapse on the corresponding lines of the salt-free system (two black lines), since for large ϕ the electric screening is dominated by the counter-ions. In Fig. 7, the low- and high-charge branches are easily distinguished. They merge continuously with each other with infinite slope at points where the system freezes at the lowest ϕ for a given C_S. Close to these points, the low- and high-charge values are similar and can be quite large, up to 10^5. In agreement with the results in Figs. 3 and 4, for $C_s < 1$ μM an iso-Z horizontal line in Fig. 7 can intersect an iso-C_S freezing line at only one ϕ value on the low-charge branch side. Additionally, there will be two phase transition points on the high-charge branch side, provided the added salt concentration C_S is low enough, so that the iso-C_s freezing line has a minimum at the intermediate concentration range of $0.01 < \phi < 0.1$. For low salt concentrations, three freezing transitions on the high-charge branch are also possible at $Z = \text{const}$. For salt concentrations higher than about 1 μM, for the iso-Z line there is one freezing transition point either on the low- or high-charge branch side.

Figure 8 depicts iso-ϕ freezing lines in the $Z-C_S$ phase diagram, showing that, for a given ϕ and C_S, there are two effective charge values allowing for freezing: One lower value for the low-charge and one larger value for the high-charge branch solution. At a constant C_S, the Z-values of the low-charge branch decrease, and those of the high charge branch increase with increasing ϕ, provided that $\phi > 0.03$. For $\phi < 0.03$, the low-charge branch values of Z still decrease with increasing C_s, whereas the high-charge values decrease within that interval until reaching a minimum charge value at $\phi \approx 0.03$. Figure 8 reveals additionally that for each volume fraction, there is a maximum salt concentration for which the

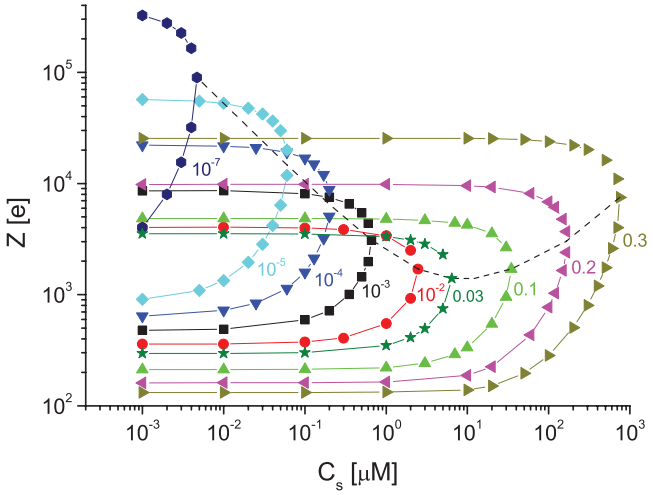

FIG. 8. RY-HV predicted iso-ϕ freezing lines in the Z–C_s phase diagram. The numbers indicate the values of ϕ. The dashed line connects the merging points of the low- and high-charge branches on the iso-ϕ lines.

system can freeze, regardless of how Z is selected. This finding can be understood from the behavior of the $S(q_m)$ vs. Z curve at constant ϕ given in Fig. 5(a), showing that for low salt content this curve crosses the horizontal HV line $S(q_m) = 3.1$ at two points, corresponding to the low- and high-charge branch charge values. With increasing salt concentration the maximum of the $S(q_m)$ vs. Z curve is decreasing, eventually becoming tangential to the horizontal HV line. This defines the largest salt concentration, at the considered ϕ, for which the system can freeze. At higher salt concentrations the system remains fluid.

Recall from Figs. 3 and 4 that for low-charge systems, the iso-charge $S(q_m)$ vs. ϕ curve crosses the horizontal HV freezing line only at a single ϕ value, while for certain higher charge systems, three ϕ values are predicted where freezing can take place. In the iso-ϕ freezing line representation in Fig. 8, this corresponds to the feature that for lower charges (lower than about 3500), there is only a single constant-ϕ freezing line going through a point of given C_S-Z coordinates, while in the higher charge region (above the dashed line in Fig. 8) there exist C_s–Z points corresponding to three different ϕ values. Thus, for an iso-Z system at sufficiently large Z, a reentrant solid–fluid transition can be traversed when ϕ is increased.

Both the low- and high-charge branch effective charges in Figs. 7 and 8 at freezing increase strongly with decreasing colloid concentration. For very low $\phi \approx 10^{-6}$ to 10^{-7} the values of both the low- and high-charge values required for freezing are of the order of 10^5e. However, it is questionable whether such large effective charge values can be attained in an experimentally realized system.

D. Universal freezing line in the $\tilde{T}$–λ phase space

So far, we have discussed freezing line diagrams in terms of experimentally controllable parameters such as C_s and ϕ. As noted in Sec. I, Yukawa-sphere systems, including the charge-stabilized colloid systems as a special case, where the

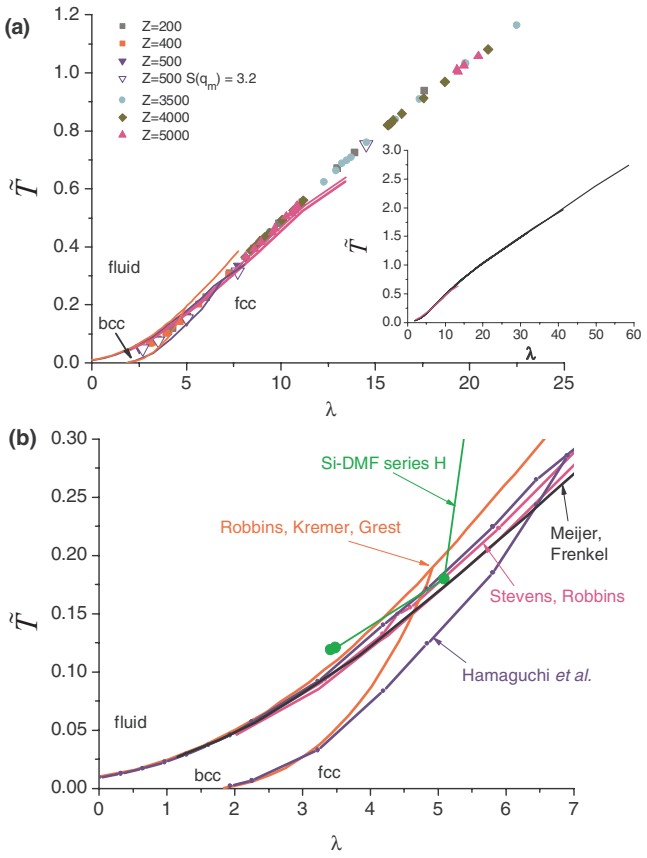

FIG. 9. (a) Universal $\tilde{T} - \lambda$ phase diagram of Yukawa particle systems with masked hard-core interactions, with data for $\lambda < 22$. The differently colored solid lines are the melting line predictions, respectively, by Meijer and Frenkel,[20] Stevens and Robbins,[22] and Hamaguchi *et al.*,[23] using the same color code as in (b). Solid symbols: RY-HV freezing point predictions using $S_f(q_m) = 3.1$. Open symbols: RY-HV predictions using $S_f(q_m) = 3.2$. Inset in (a) shows all RY-HV calculated freezing points corresponding to the results shown in Figs. 6 and 7. A very broad range of λ values is covered here. (b) Magnified lower-values λ part of the phase diagram, showing in addition the experimental results for the H-series system of silica spheres in DMF (in green).

physical hard core plays no role, are fully characterized in their equilibrium phase behavior by two dimensionless parameters, namely, the reduced screening parameter, $\lambda = \kappa \langle r \rangle$, and the reduced temperature $\tilde{T} = k_B T / u(\langle r \rangle)$. The latter parameter is a measure of the thermal energy relative to the pair energy at the (simple-cubic) next-neighbor distance $\langle r \rangle$. As thoroughly discussed in Refs. 19, 20, 22, and 23, there exists a universal $\tilde{T} - \lambda$ phase diagram where systems of equal λ and $\tilde{T}$ share the $S(q)$ and $g(r)$, when $\langle r \rangle$ is selected as the length unit.

Figure 9(a) displays this universal $\tilde{T} - \lambda$ phase diagram, including our RY-HV calculated freezing points (solid symbols), for systems of different effective charge values as given in the figure. Also systems with varying amounts of added salt are considered (cf. Fig. 4) and, in addition, a number of RY-HV based freezing points attained for a slightly larger HV freezing value of $S_f(q_m) = 3.2$ (open symbols). This serves to demonstrate that the universal freezing line is insensitive to smaller changes in selected HV peak value. The freezing line predicted by our RY-HV based data is in remarkably good overall agreement with the melting line predictions by

Meijer and Frenkel (MF),[20] and Stevens and Robbins (SR),[22] and also with the more recent and more accurate MD simulation results for the melting line by Hamaguchi *et al.*[23]

In principle, one needs to distinguish the melting line from the freezing line, with the latter located somewhat above the former.[25,26,40] However, the difference between the two lines is quite small for smaller values of λ (small miscibility gap). This is illustrated in Figs. 9(a) and 9(b), showing both the melting and freezing lines predictions of Stevens and Robbins.[22] In the one-component plasma limit of zero electric screening, for which $\tilde{T}(\lambda = 0) = 9.383\times10^{-3}$, the density difference between coexisting bcc and fluid phases becomes exactly zero, i.e., there is an isochoric transition.[23] We emphasize here that our RY-HV based results cover a large range of λ values, extending well beyond that explored earlier by Meijer and Frenkel,[20] Stevens and Robbins,[22] and Hamaguchi *et al.*.[23]

Figure 9(b) magnifies the lower-λ part of the phase diagram, which includes the bcc phase region. It displays the original melting line prediction by Robbins, Kremer, and Grest (RKG),[16] in comparison to the more recent MD simulation results by Hamaguchi *et al.*[23] According to Hamaguchi *et al.*, the triple point of three-phase bcc-fcc-fluid coexistence is located at $(\tilde{T}_t,\ \lambda_t) = (0.2856,\ 6.90)$, i.e., at a screening value λ substantially larger than that predicted by RKG. According to Fig. 9(b), the RKG melting line overestimates the melting temperature and thus the crystal stability. In the figure, we show additionally the state point of the 5 μM system of our silica in DMF H series (solid green points to the right) which will be addressed further down. This state point is located inside the bcc pocket region predicted by Hamaguchi *et al.*, but outside the RGK predicted bcc region. Only the bcc phase space pocket by Hamaguchi *et al.* is in accord with our experimental findings of a bcc crystal structure for this system (see Fig. 12).

In Fig. 10, we depict the $(\tilde{T} - \lambda)$ phase-space trajectory traversed with increasing ϕ by the high-charge ($Z = 5000$) and "zero-salinity" ($C_s = 10^{-9}$ M) concentration series, whose RY structure factors have been presented already in Fig. 2. The complex shape of this trajectory, which intersects the freezing/melting lines three times, results from the non-monotonic ϕ-dependence of the parameters $\tilde{T}$ and λ shown in the inset.

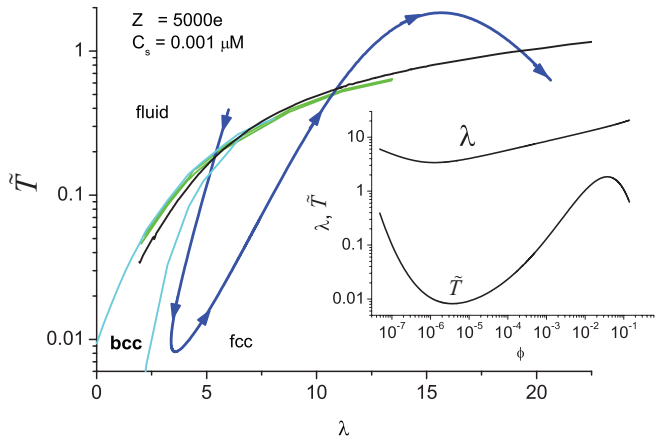

FIG. 10. $\tilde{T} - \lambda$ phase-space trajectory of the high-charge, zero-salinity concentration series system of Fig. 2(b) (blue solid line). The arrows on the blue line indicate the direction of increasing ϕ. The trajectory starts in the fluid phase at an extremely low concentration $\phi \sim 10^{-8}$, crossing next the bcc and then the fcc crystal phase at around $\phi = 6.82\times10^{-8}$, returning to the fluid phase at $\phi = 4.39\times10^{-3}$, and finally crossing into the fcc phase at $\phi \sim 0.10$. Inset: ϕ dependence of λ and $\tilde{T}$ along the trajectory.

E. Salt-induced fluid-bcc-fluid reentrant transition: Experimental results

From an experimental viewpoint, it is of interest to study the freezing lines also in the (Z–C_s) phase diagram for systems of a given ϕ. We consider here two volume fractions, namely, $\phi = 0.077$ and $\phi = 0.14$. In recent x-ray experiments,[10] we have studied silica in DMF systems at these two volume fractions as a function of C_s. As in our earlier work, we refer to them here as the added salt series H ($\phi = 0.077$) and K ($\phi = 0.14$).

Consider in Fig. 11 first the lower-concentrated system at $\phi = 0.077$. The lower (upper) part of the freezing line for the low-charge (high-charge) branch systems is determined by the RY-HV scheme using $S_f(q_m) = 3.1$ (solid and open squares). According to the RY-HV rule, a homogeneous fluid phase exists only outside the region bounded by the two freezing line parts. For $C_s > 20$ μM, no solid phase is predicted for any value of the effective charge.

In comparing the interconnected low- and high-charge freezing lines for $\phi = 0.14$ (open and solid diamonds—series K) with those for $\phi = 0.077$ (open and solid squares—series H), one notices from Fig. 11 that for the more concentrated K series systems the RY-HV predicted freezing values for Z are located at lower (larger) values on the low-charge (high-charge) branch of the freezing line. Thus, the crystalline

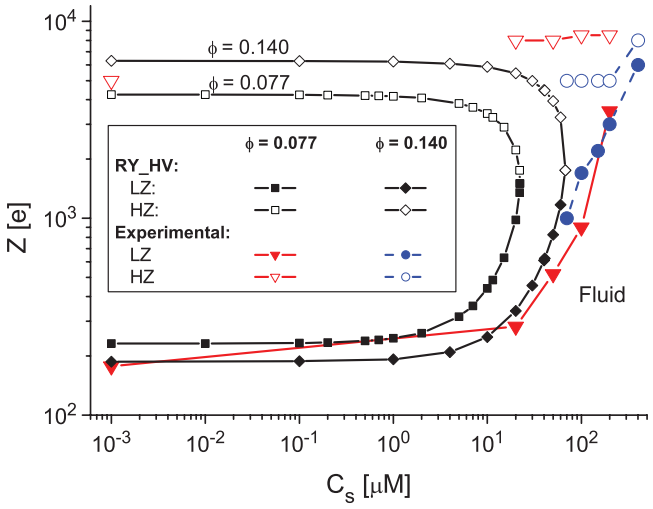

FIG. 11. Squares (diamonds) connected by straight line segments: RY-HV freezing line in the Z–C_s phase diagram for $\phi = 0.077$ ($\phi = 0.140$), obtained using $S_f(q_m) = 3.1$. Solid and open symbols represent low- and high-charge freezing values of Z, respectively. Solid (open) red triangles: values of $Z(C_s)$ obtained from a RY-fit to the experimental $S(q)$ for the systems of series H ($\phi = 0.077$) in Ref. 10 using the low- (high-) charge branch solution. Solid (open) blue circles: values of $Z(C_s)$ obtained from a RY-fit to the experimental $S(q)$ for the systems of series K ($\phi = 0.14$) in Ref. 10 using the low- (high-) charge branch solution.

region of the phase diagram is broader for the more concentrated C_s series, where crystallization is predicted to be absent for any Z when $C_s > 68$ μM. The lowest experimentally studied C_s value for the series K fluid systems studied in Ref. 10 was 70 μM.

Figure 11 displays additionally the salinity dependence of the low- and high-charge values of Z in the experimental salinity series H ($\phi = 0.077$) and K ($\phi = 0.14$) within the fluid regime which have been studied earlier in Ref. 10 by x-ray synchrotron radiation scattering. The effective charge in both series was determined from a RY fit to the experimental $S(q)$. The experimental trajectories (triangles and circles) for $Z(C_s)$ extend over an added LiCl concentration range of 10^{-3} to 10^2 μM (Series H) and 70–400 μM (Series K). The effective charge of the low-charge branch RY solution for both series increases monotonically with increasing salt concentration, rather slowly at low salinity but quite steeply at higher salt content.

The results for $Z(C_s)$ in Fig. 11, obtained from the RY fits to experimental $S(q)$ using the high-charge branch Z solutions (open triangles), show a very weak C_s dependence for both experimental series. Within the experimental errors, the RY fits of $S(q)$ are equally good for both branches, so that it is not possible to decide on the basis of these fits alone whether the low- or high charge values is assumed in the experimental system. The explored series K systems at high salt content ($C_s > 100$ μM) are interesting also from the point of view that in this salinity region the low-charge and high-charge solutions for Z become nearly equal so that the distinction between the low- and high-charge solutions ceases.

The behavior of the low-charge freezing lines $Z_{\text{low}}(C_s)$ in Fig. 11 is consistent with Poisson-Boltzmann theory based charge-renormalization calculations which predict an increasing effective Z with increasing salt concentration. The experimental trajectory in Fig. 11 of series H suggests, for salt concentrations of the order of 1 μM, a reentrant fluid-crystal-fluid transition, with the system being in a fluid state at low C_s and Z. According to the experimental C_s–Z trajectory (solid red points), Z increases sufficiently strongly with C_s that crystallization is induced, at a value of C_s roughly in the region of 1 μM. With further increasing C_s (and Z), the screening effect by the surface-released counterions becomes so strong that the crystalline system melts again.

While our experimental study in Ref. 10 was focused on silica spheres in DMF systems located in the fluid phase regime, a few samples have shown clear evidence of crystalline order. An example of SAXS scattering data obtained for a $C_s = 5$ μM sample of the H series, which was not discussed in Ref. 10 is given in Fig. 12. In this figure, symbols (solid circles) represent the experimental static structure factor data, and the dashed line corresponds to a fluid-like RY structure factor, calculated using parameters interpolated from the neighboring liquid points of series H.[10] The solid curve depicts the difference values between the experimental and RY-calculated structure factors.

From this difference curve, one can immediately recognize the presence of additional experimental peaks at $q \approx 0.020$, 0.029, and 0.035 nm^{-1}, and a broad peak located in between $q = 0.037$ nm^{-1} and 0.045 nm^{-1}. The positions

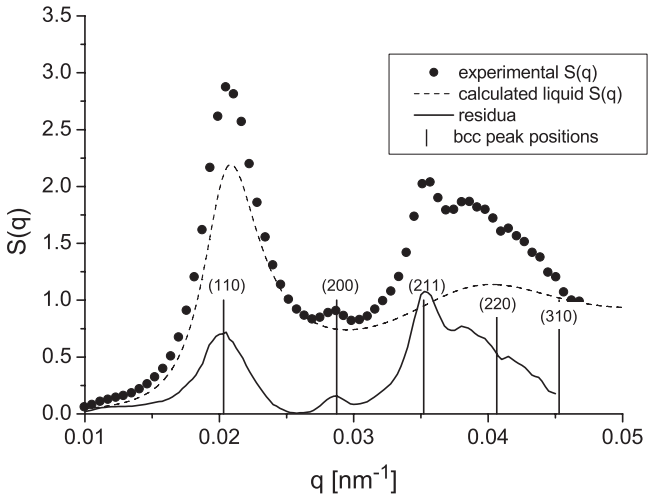

FIG. 12. Experimental SAXS structure factor (solid circles), RY calculated fluid-system $S(q)$ (dashed curve), and their difference values (solid curve), for the 5 μM salt content sample of series H. The vertical line segments indicate the wavenumber locations of the first few bcc lattice vectors (with Miller indices).

of these peaks can be nicely interpreted as the Bragg peak positions of a bcc crystal. The bcc Bragg peak locations are indicated in Fig. 12 by vertical line segments, labeled by the corresponding Miller indices. This finding allows us to interpret the (solid) difference line as the excess intensity due to the diffraction pattern from the crystalline part of the sample. The Bragg peaks are broadened by crystal imperfections and their limited size (Scherrer width). Their intensities cannot be compared since they depend on the colloid-crystal orientation with respect to the incident beam which cannot be controlled for a polycrystalline sample. Additionally, the experimental system was optimized for the measurements of the x-ray photon correlation spectroscopy (XPCS) correlation functions. For this purpose, a point detector was used, with the consequence that a full detection in reciprocal space has not been possible. However, the positions of the peaks on the wavenumber axis, clearly indicative here of a bcc structure, are not affected.

It is interesting to note from Fig. 12 that the principal peak of the RY-$S(q)$, and the first Bragg peak are partially overlapping. In fact, if there wouldn't be other Bragg peaks visible, one could be tempted to interpret the main experimental peak at $q \approx 0.020$ as the principal peak of a purely fluid-like $S(q)$, so that from a RY structure factor fit one would obtain a different effective charge value. We have assumed here that the charge value at $C_s = 5$ μM can be obtained by an interpolation from the charge values determined from the RY structure factor fits at $C_s = 0$ and 20 μM, respectively, where at both salt concentrations the sample was found to remain fluid-like disordered. For the reasons given in the preceding paragraph, another scattering experiment of the same sample at different positions could result in a much higher or lower principal peak height, depending on the point detector path with respect to the Bragg peaks positions.

The $\tilde{T}-\lambda$ trajectories of the experimental silica colloids in DMF systems of series H and K ($\phi = 0.077$ and 0.14,

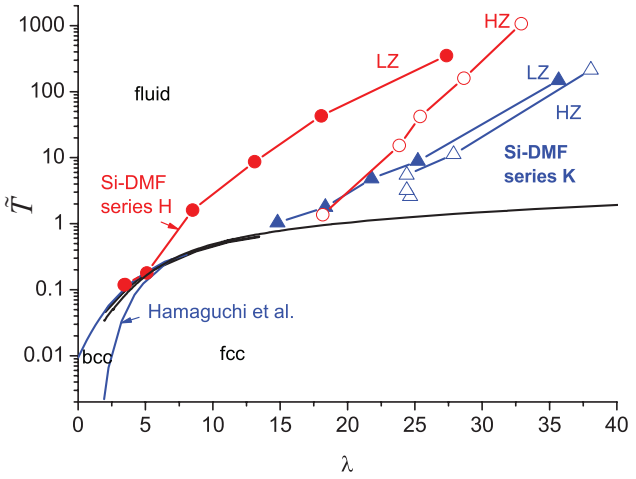

FIG. 13. System trajectories of the H (red symbols) and K series (blue symbols) in the universal $\tilde{T}-\lambda$ phase diagram obtained by Hamaguchi *et al.*[23] The black freezing line extending beyond the one of Hamaguchi *et al.* is composed of the freezing points presented in Figs. 6–8. "LZ" and "HZ" denote the low- and high-charge branch solutions, respectively.

respectively), where the added salt (LiCl) concentration is varied, are shown in Fig. 13. For both added salt series, the trajectories of the low- and high-charge branches (denoted by LZ and HZ, respectively) are clearly different. Regarding the H-series systems, the LZ-trajectory starts at low λ (salt-free case) in the fluid phase. Subsequently, at $\lambda \approx 5$ ($C_S \approx 5\ \mu$M), it enters the bcc crystal phase just to quickly return back into the fluid phase at slightly larger λ. Thus, a reentrant fluid–solid–fluid transition is experimentally observed indeed. The bcc structure of the crystal at $\lambda \approx 5$ is corroborated by the SAXS Bragg peaks positions in Fig. 12, characteristic of a bcc crystal.

In Fig. 13, no reentrant behavior is observed in contrast to the HZ trajectory of the H-series (open red circles), which tends towards the fcc phase with decreasing λ (decreasing salt concentration). It is interesting to note that the lowest data point of this HZ trajectory corresponds to the salt-free sample represented in Fig. 11 by the open triangle at $C_S = 10^{-3}\ \mu$M.

The low- and high-charge trajectories of the experimental K series are qualitatively similar. Both trajectories approach the fcc crystal with decreasing λ (decreasing salt), however, showing no reentrant transition. The LZ trajectory of series K starts very close to the freezing line predicted by Hamaguchi *et al.*[23] The first data point corresponds to the lowest salt concentration ($C_S = 70\ \mu$M) for which the sample was observed to become fluid. For lower salt concentrations, the K-series samples were found to be crystalline with an fcc structure.

IV. CONCLUSIONS

Freezing lines of charge-stabilized colloidal systems described by a Yukawa-type repulsive pair potential have been constructed, based on the accurate Rogers-Young integral equation scheme for $S(q)$ in conjunction with the empirical Hansen-Verlet rule for the onset of freezing.

To facilitate the comparison with experiments where the phase behavior of charge stabilized systems is of interest, freezing lines involving experimentally controllable parameters were discussed in the C_s–ϕ, Z–ϕ, and Z–C_s phase spaces. These two-parameter freezing-line diagrams, where a respective third parameter is varied, should be very useful for the systematic planning of experiments, and for understanding the role played by different parameters in defining the solid or fluid phase states of charged colloids. For this purpose, the RY-HV based freezing lines have been constructed over a vast parameter range, not attainable by exceedingly more time consuming computer simulations.

On accounting for the fact that from an experimental viewpoint practically indistinguishable $S(q)$s are obtained for in general two distinctly different effective charge values, namely, the low-charge and high-charge branch values, respectively, both branches of the two-parameter freezing lines have been discussed to obtain a complete description.

A possible way to distinguish whether a particular experimental Yukawa-type system assumes its low- or high-charge Z value, is to determine the lattice type of the resulting crystal: The majority of low-charge systems will freeze into a bcc solid, but freezing into an fcc solid (according to the RY-HV scheme) can be also observed for high salinities. In contrast, in high-charge branch systems where values $\lambda > 6.9$ are always found, freezing takes place only into a fcc solid. An additional criterion which can be used to identify the actual, experimentally occurring effective charge, provided the low-charge and high-charge values are largely different, are charge condensation/regulation considerations which give upper bounds to the experimentally realizable effective charge.

The universal $T-\lambda$ freezing line traced out by our RY-HV results for $S(q_m) = 3.1$, is in good agreement with earlier simulation-based freezing and melting line predictions by various groups,[16,19,20,22,23] thereby extending this line to a largely extended range of λ values. We have checked that the universal freezing line is quite insensitive to small changes in the HV freezing value. Here, we re-emphasize that only systems with hard-core interactions masked by the electric repulsion have been considered, representative for most charge-stabilized systems.

The RY-HV based two-parametric space freezing lines have been used to analyze the system trajectories of two silica in DMF systems, one at $\phi \approx 0.077$ (series H) and the other at $\phi \approx 0.14$ (series K). Both the systems were studied using SAXS as functions of added monovalent salt. We have shown experimentally, and in accord with the phase diagram calculations by Hamaguchi *et al.*[23] and our RY-HV based Z–C_s phase diagram in Fig. 11, that a re-entrant fluid-solid-fluid transition takes place for the series H systems at constant colloid concentration, when the salt concentration is increased.

In the work by Royall *et al.*,[6] a similar reentrant fluid – bcc−fluid transition has been observed experimentally for charged PMMA spheres in a solvent mixture as the volume fraction was increased. The unusual part in this sequence is the reentrant melting at a larger ϕ. Royall *et al.* explain this sequence essentially by the strong ϕ dependence of the effective colloid charge which, in the considered concentration range, decreases with an increasing ϕ. For the silica in DMF system discussed in Fig. 11, a fluid–bcc–reentrant fluid transition sequence is observed instead for increasing salt

concentration at constant ϕ. Here, the unusual part in the sequence is the freezing upon increasing salt concentration, in apparent conflict with the frequently observed behavior in charged colloidal suspensions where the systems stays fluid when the salt concentration C_s is increased (at fixed ϕ). As discussed before, the increase of Z with increasing salt concentration in our silica in DMF system (via a weakening counterion condensation) is sufficiently strong to induce crystallization. Thus, in both the reentrant transition scenarios, the unusual parts are explained by the respective parameter dependence of the effective charge: a falling $Z(\phi)$ in the case of,[6] and a rising $Z(C_s)$ for silica in DMF.

In place of the HV freezing criterion, one could have used the dynamic freezing criterion by Löwen *et al.*,[5] on the ratio of long-time to short-time self-diffusion coefficients, $D_L/D_S = 0.1$, at freezing (LPS criterion, for short), to map out the fluid−solid freezing line, as done for dusty plasmas in the simulation work by Vaulina and Khrapak.[24] However, different from dusty plasmas, the non-Newtonian and over-damped dynamics of colloids is subject to long-ranged hydrodynamics interactions. While fast and accurate analytic methods exist for calculating D_S in the presence of hydrodynamic interactions,[41] a precise calculation of the long-time coefficient, D_L, is still very demanding and time-consuming up to the present day. For colloids, it would thus be highly uneconomical to derive a freezing line from calculations of D_L in conjunction with the LPS criterion. Moreover, as shown by one of the present authors[42] for the important case of colloidal (low-salinity) systems in the weak screening regime, there exists a one-to-one mapping between the static HV and the dynamic LPS criterion of colloidal freezing.

Finally, we note that the behavior and the physical interpretation of the colloid-colloid pair energy in Yukawa sphere systems in relation to the pair structure and the $\widetilde{T}-\lambda$ freezing line will be discussed in the forthcoming paper II.

ACKNOWLEDGMENTS

G.N. acknowledges support by the Deutsche Forschungsgemeinschaft (SFB-TR6, project B2) and helpful discussions with M. Heinen and A.J. Banchio. Partial support by the "SoftComp" Network of Excellence (Grant No. S080118) is gratefully acknowledged. Partial support by the Polish National Science Centre (Grant No. 2011/01/B/ST3/02271) is gratefully acknowledged. J.G. acknowledges partial support by the Human Capital Operating Program, Project 4.1.1 for the Faculty of Physics, Adam Mickiewicz University Poznan, Poland. The experimental data in Fig. 12 were obtained by SAXS experiments at ESRF reported in Ref. 10, in cooperation with J. Buitenhuis, P. Holmqvist, P. Lettinga, and G. Meier (Reseach Centre Jülich, Germany). We thank them for their permission to show these data in the present paper.

[1] D. Riese, G. Wegdam, W. Vos, R. Sprik, D. Fenistein, J. Bongaerts, and G. Grübel, Phys. Rev. Lett. **85**, 5460 (2000).
[2] W. Härtl, C, Beck, and R. Hempelmann, J. Chem. Phys. **110**, 7070 (1999).
[3] L. F. Rojas-Ochoa, C. Urban, P. Schurtenberger, T. Gisler, and H. H. von Grünberg, Europhys. Lett. **60**, 802 (2002).
[4] L. F. Rojas-Ochoa, R. Castaneda-Priego, V. Lobaskin, A. Stradner, F. Scheffold, and P. Schurtenberger, Phys. Rev. Lett. **100**, 178304 (2008).
[5] H. Löwen, T. Palberg, and R. Simon, Phys. Rev. Lett. **70**, 1557 (1993).
[6] C. P. Royall, M. E. Leunissen, A.-P. Hynninen, M. Dijkstra, and A. van Blaaderen, J. Chem. Phys. **124**, 244706 (2006).
[7] W. B. Russel, D. A. Saville, and W. R. Schowalter, *Colloidal Dispersions* (Cambridge University Press, Cambridge, 1989).
[8] A. J. Banchio, J. Gapinski, A. Patkowski, W. Haeußler, A. Fluerasu, S. Saccana, P. Holmqvist, G. Meier, M. P. Lettinga, and G. Nägele, Phys. Rev. Lett., **96**, 138303 (2006).
[9] J. Gapinski, A. Patkowski, A. Banchio, P. Holmqvist, G. Meier, M. P. Lettinga, and G. Nägele, J. Chem. Phys. **126**, 104905 (2007).
[10] J. Gapinski, A. Patkowski, A. J. Banchio, J. Buitenhuis, P. Holmqvist, M. P. Lettinga, G. Meier, and G. Nägele, J. Chem. Phys. **130**, 084503 (2009).
[11] P. Holmqvist and G. Nägele, Phys. Rev. Lett. **104**, 058301 (2010).
[12] W. Häussler and B. Farago, J. Phys. Condens. Matter **15**, S197 (2003).
[13] J. Gapinski, A. Wilk, A. Patkowski, W. Häussler, A. J. Banchio, R. Pecora, and G. Nägele, J. Chem. Phys. **123**, 054708 (2005).
[14] F. Roosen-Runge, M. Hennig, F. Zhang, R. M. J. Jacobs, M. Sztucki, H. Schober, T. Seydel, and F. Schreiber, Proc. Natl. Acad. Sci. U.S.A. **108**, 11815 (2011).
[15] A F. Zhang, M. W. A. Skoda, R. M. J. Jacobs, R. A. Martin, C. M. Martin, and F. Schreiber, J. Phys. Chem. B **111**, 251 (2007).
[16] O. Robbins, K Kremer, and G. S. Grest, J. Chem. Phys. **88**, 3286 (1988).
[17] A.-P. Hynninen and M. Dijkstra, J. Phys. Condens. Matter **15**, S3557 (2003).
[18] M. Heinen, P. Holmqvist, A. J. Banchio, and G. Nägele, J. Chem. Phys. **134**, 044532 & 129901 (2011).
[19] K. Kremer, M. O. Robbins, and G. S. Grest, Phys. Rev. Lett. **57**, 2694 (1986).
[20] E. J. Meijer and D. Frenkel, J. Chem. Phys. **94**, 2269 (1991).
[21] E. J. Meijer and F. El Azahar, J. Chem. Phys. **106**, 4678 (1997).
[22] M. J. Stevens and M. O. Robbins, J. Chem Phys. **98**, 2319 (1993).
[23] S. Hamaguchi, R. T. Farouki, and D. H. E. Dubin, Phys. Rev. E **56**, 4671 (1997).
[24] O. S. Vaulina and S. A. Khrapak, J. Exp. Theor. Phys. **92**, 228 (2001).
[25] D. C. Wang and A. P. Gast, J. Phys. Condens. Matter **11**, 10133 (1999).
[26] D. C. Wang and A. P. Gast, J. Chem. Phys. **112**, 2826 (2000).
[27] A.-P. Hynninen and M. Dijkstra, Phys. Rev. E **68**, 021407 (2003).
[28] P. N. Pusey, in: *Liquids, Freezing and Glass Transition*, Les Houches Sessions 1989, edited by J.-P. Hansen, D. Levesque, and J. Zinn-Justin (North-Holland, Amsterdam, 1991), pp. 763–942.
[29] T. V. Ramakrishnan and M. Yussouf, Phys. Rev. B **19**, 326 (1979).
[30] T. V. Ramakrishnan, Phys. Rev. Lett. **48**, 541 (1982).
[31] J.-P. Hansen and L. Verlet, Phys. Rev. **184**, 151 (1969).
[32] J. Gapinski, A. Patkowski, G. Nägele, J. Chem. Phys. **132**, 054510 (2010).
[33] S. Alexander, P. M. Chaikin, P. Grant, G. J. Morales, and P. Pincus, J. Chem. Phys. **80**, 5776 (1984).
[34] S. Pianegonda, E. Trizac, and Y. Levin, J. Chem. Phys. **126**, 014702 (2007).
[35] T. E. Colla, Y. Levin, and E. Trizac, J. Chem. Phys. **131**, 074115 (2009).
[36] F. Smallenburg, N. Boon, M. Kater, M. Dijkstra, and R. van Roij, J. Chem. Phys. **134**, 074505 (2011).
[37] A. P. dos Santos, A. Diehl, and Y. Levin, J. Chem. Phys. **123**, 104105 (2010).
[38] F. J. Rogers and D. A. Young, Phys. Rev. A **30**, 999 (1984).
[39] A. J. Banchio and G. Nägele, J. Chem. Phys. **128**, 104903 (2008).
[40] H. Graf and H. Löwen, Phys. Rev. E **57**, 5744 (1998).
[41] M. Heinen, A. J. Banchio and G. Nägele, J. Chem. Phys. **135**, 154504 (2011).
[42] G. Nägele, M. Kollmann, R. Pesche, and A. J. Banchio, Mol. Phys. **100**, 2921 (2002).